



HAL
open science

Structural characterization of ultrathin Cr-doped ITO layers deposited by double-target pulsed laser ablation

Maura Cesaria, Anna Paola Caricato, Gilberto Leggieri, Armando Luches, Maurizio Martino, Giuseppe Maruccio, Massimo Catalano, Maria Grazia Manera, Roberto Rella, Antonietta Taurino

► **To cite this version:**

Maura Cesaria, Anna Paola Caricato, Gilberto Leggieri, Armando Luches, Maurizio Martino, et al.. Structural characterization of ultrathin Cr-doped ITO layers deposited by double-target pulsed laser ablation. *Journal of Physics D: Applied Physics*, 2011, 44 (36), pp.365403. 10.1088/0022-3727/44/36/365403 . hal-00651640

HAL Id: hal-00651640

<https://hal.science/hal-00651640>

Submitted on 14 Dec 2011

HAL is a multi-disciplinary open access archive for the deposit and dissemination of scientific research documents, whether they are published or not. The documents may come from teaching and research institutions in France or abroad, or from public or private research centers.

L'archive ouverte pluridisciplinaire **HAL**, est destinée au dépôt et à la diffusion de documents scientifiques de niveau recherche, publiés ou non, émanant des établissements d'enseignement et de recherche français ou étrangers, des laboratoires publics ou privés.

Structural characterization of ultrathin Cr-doped ITO layers deposited by double target pulsed laser ablation

Maura Cesaria¹, Anna Paola Caricato¹, Gilberto Leggieri¹, Armando Luches¹, Maurizio Martino¹, Giuseppe Maruccio^{1,2}, Massimo Catalano³, Maria Grazia Manera³, Roberto Rella³ and Antonietta Taurino^{3,a)}

¹*Physics Department, University of Salento, Via Arnesano, 73100 Lecce, Italy*

²*NNL Istituto Nanoscienze-CNR, Via Arnesano, 73100, Lecce, Italy*

³*Institute for Microelectronics and Microsystems, IMM-CNR, Via Monteroni, 73100 Lecce, Italy*

Abstract

In this paper we report on the growth and structural characterization of very thin (20nm) Cr-doped ITO films, deposited at room temperature by double target pulsed laser ablation on amorphous silica substrates. The role of Cr atoms into the ITO matrix is carefully investigated at increasing doping content by transmission electron microscopy (TEM). Selected area electron diffraction, conventional bright field and dark field as well as high resolution TEM analyses, and energy dispersive x-ray spectroscopy demonstrate that (i) crystallization features occur even despite the low growth temperature and thin thickness, (ii) no chromium or chromium oxide secondary phases are detectable, regardless of the film doping levels, (iii) the films crystallize as crystalline flakes forming large angle grain boundaries; (iv) the observed flakes consist of crystalline planes with local bending of the crystal lattice. Thickness and compositional information about the films are obtained by Rutherford back-scattering spectrometry. Results are discussed by invoking the combined effects of growth temperature, smaller ionic radius of the Cr cation compared to the trivalent In ion, doping level, film thickness, double-target doping technique and peculiarities of the pulsed laser deposition method.

PACS: 68.37.Lp, 81.15.Fg, 68.55.Ln, 68.60.Bs

^{a)} E-mail address: antonietta.taurino@le.imm.cnr.it

Introduction

Degenerate wide band gap oxide semiconductors recently attracted large interest as promising host compounds for diluted magnetic semiconductors (DMSs) [1,2] with high Curie temperature for room temperature spintronic applications, ranging from logic circuits to spin-LED devices allowing polarized emission [3-10]. In this context, indium tin oxide (briefly ITO) [11] is a very interesting material due to its good opto-electronic properties, good adaptability to be interfaced with known semiconductor/electronic materials, and indications suggesting RT carrier-mediated ferromagnetism in Cr-doped indium oxide films [12].

In the general framework of DMSs, a theoretical comprehensive model able to explain the basic mechanisms leading to ferromagnetism is unavailable and different results are reported even for the same composition and depending on the growth technique. A key point is the relationship between magnetic order and dopant uniformity and/or clustering above the solubility limit of the magnetic dopant in the host matrix [1, 13]. In this respect, the drawback of low solubility of a magnetic element can be overcome by non-equilibrium growth techniques, such as Pulsed Laser Deposition (PLD) [1,14-16]. In addition, thin films grown by PLD exhibit higher performances and better structural characteristics compared to other equilibrium deposition techniques [17-19].

Generally, avoiding the formation of dopant oxides and dopant oxide segregation at the grain boundaries (GBs) within the growing film necessitates of carefully tuned deposition conditions. Therefore, the growth of Cr-doped ITO films is not a straightforward issue and a controlled growth method is required in order to obtain films with tunable magneto-opto-electronic properties. Moreover, since growth techniques and parameters strongly affect film properties through the involved structural features, the investigation of the resulting film microstructure is of paramount importance to tune growth evolution and to understand the correlation between film microstructure and its macroscopic opto-electronic properties. Therefore, a direct control of the morphological features of the films is required.

According to this, the present paper focuses on the investigation of the structural properties of very thin Cr-doped ITO films grown by the double target PLD approach. The characterization of ITO films

is not considered in this paper because already widely investigated in the literature [20-29]. Samples as thin as 20 nm were grown on amorphous silica substrates at room temperature. Two different doping levels were considered and compared. A very low film thickness was chosen to investigate the effect of Cr insertion into ITO, devoting particular attention to growth kinetics, occurrence of different phases and structural evolution induced by the dopant content. In fact, PLD-induced growth hyper-thermal-conditions and high density of nucleation sites, doping-promoted heterogeneous nucleation and changes of the film microstructure and morphology related to Cr-induced strain effects are expected to strongly influence the initial growth and the structural characteristics of the films. Indeed, the first few tens of nanometers act as seed coating, which critically determines the features of the growing and final film. In this respect, substrate nature and surface are important parameters in determining the initial film nucleation stage and the crystallization. The subsequent growth favors the surface coverage and transformation of the amorphous phase to the crystalline one, coalescence of the islands, increasing grain size and crystallinity as well as strain relaxing beyond the critical thickness.

The doping process by PLD can be accomplished by using several approaches such as ablation of a single target obtained by premixing of the materials to be deposited [30,31], ion implantation [32], dual beam method [33-37], dual target simultaneous PLD apparatus [38] and switching ablation among targets with different composition. It must be emphasized that the microstructure of the pellet material strongly affect the final film morphology and structural quality through the formation, distribution and density of particulates in the deposit [39-42]. In this respect, ablation by a single premixed multi-elemental pellet has significant limitations and drawbacks in target density, fixed concentration of dopant, inability to change *in situ* the doping conditions during the deposition process, differential scattering in the plume itself among species with very different masses that can induce incorrect film stoichiometry and non uniform dopant distribution as well as cluster or secondary phases of the dopant oxide in the oxygen background atmosphere.

The approach based on periodic switching of the laser beam between sintered ITO and metallic Cr targets was our choice due to the following reasons: i) a priori minimization of the formation of clusters and dopant oxide phases thanks to the high purity of the metallic dopant target compared to a single premixed multi-elemental sintered pellet, ii) independent ablation of the targets that avoids any

interaction among the ablated species during the plasma plume expansion and possibly enables to ablate the dopant metallic target in oxygen-free background atmosphere, and iii) low costs and possibility to finely control *in situ* the dopant localization and amount by changing the ratio between the number of laser pulses on each target.

Experimental details

Cr-doped ITO (20 nm) films were deposited by PLD using a Lambda Physics 305i ArF excimer laser ($\lambda = 193\text{nm}$, $\tau = 20\text{ns}$) on amorphous silica substrates held at room temperature. No post-annealing treatment was carried out. Whereas the amorphous nature of the chosen substrate can delay the onset of the crystalline phase, it avoids the strain effects and driven growth commonly induced by mismatched and oriented substrates.

Figure 1 sketches the PLD experimental set-up composed of i) a stainless steel vacuum chamber, ii) a UV laser source with associated beam delivery optics, iii) a combined rotative-turbo pump system, iv) a mechanism to inject gas within the chamber during reactive PLD, v) a target holder equipped with a computer controlled multi-target carousel mechanism which enables the *in situ* interchange of the two targets and the rotation of each target around its own axis. The laser beam was incident at 45° with respect to the target surface. Before starting the film deposition, the chamber was evacuated down to a background pressure as low as $\sim 10^{-5}$ Pa. Then a dynamic flow of molecular oxygen was injected in the deposition chamber, resulting in a background pressure of 1 Pa for ITO deposition. The Cr ablation was performed in a background pressure of 10^{-3} Pa. In order to clean the target surface before the deposition, a shutter was placed between the substrate and the target to avoid contamination of the substrate and a few thousands of laser pulses were focused on the target at 10Hz. In order to avoid any contamination problem both targets were encapsulated with a stainless steel cylindrical cup. In such a way only one target at once was exposed to the laser beam and to the backscattered elements.

Commercially available sintered ITO, with weight composition of 90% In_2O_3 and 10% SnO_2 , and metallic Cr pellets were used as ablation targets. During the laser-target interaction, the pellets were continuously rotated to avoid the drilling and damaging of the material to be ablated at the same target

position. All depositions were carried out at a laser fluence of 4 J/cm^2 and at a target-substrate distance of 55 mm. The repetition rate of the laser pulses was set to 1 Hz for both ITO and metallic Cr. The Cr insertion within the ITO matrix was accomplished by periodically switching the ablating laser between the ITO and Cr target. Several switching cycles were needed to obtain the desired thickness of the doped films. Two dopant concentrations were obtained by changing the total ablation time on each target, which will be referred later on as low-doping (LD) and high-doping (HD), respectively. The ratio between the number of pulses on the Cr target and the number of pulses on the ITO target was 0.1 for the LD and 0.4 for the HD, respectively.

Concerning the used doping technique, the following remarks can be inferred.

The independent ablation of the two targets and the choice of the number of laser pulses allows to achieve finely tuned doping levels. Then, the very different and tunable pulse numbers on the two targets avoid the formation of dopant or dopant oxide multilayers.

The PLD technique favors the dopant migration and dilution thanks to the pulsed nature of the PLD deposition-flux and the hyper-thermal energetic distribution of the laser-produced plasma, which is tunable either by the laser fluence or by the background pressure and composition in the deposition chamber [15-18], at fixed laser fluence. Moreover, the independent ablation of the targets avoids any gas-phase interaction between the different species composing the ITO and the Cr targets and allows ablation of the dopant metallic target in oxygen-free background atmosphere. This feature minimizes the formation of clusters and dopant oxide phases during the plasma plume expansion.

Finally, since target interchange, positioning and rotation are adjustable from outside the deposition chamber by a computer-controlled stepper motor, the internal conditions of the deposition chamber, namely clean atmosphere and background pressure, are fully preserved in each step and doping content is finely tunable *in situ*.

Based on the above discussion, the choice of the described deposition approach is expected to be the best-suited to dope ITO films with Cr even for room temperature growth.

The films were deposited on $\langle 100 \rangle$ Si substrates and on carbon coated Cu grids for Rutherford back scattering (RBS) and transmission electron microscopy (TEM) investigations, respectively.

Film morphology, crystal structure, and chemical composition of the films deposited on Cu grids were examined by plan-view TEM analyses; in particular, a Leo 922 Transmission Electron Microscope, operating at an accelerating voltage of 200 kV was used for bright field/dark field as well as for selected area electron diffraction (SAED) investigations. High resolution analyses and chemical investigations by energy dispersive X-ray spectroscopy (EDS) were performed by using a Tecnai G2 instrument, operating at 300 kV.

The nominal film thickness was first controlled by means of the total numbers of laser pulses and the target-substrate distance. Rutherford backscattering spectrometry (RBS) with 2.2 MeV He⁺ ions at 160° scattering angle was used to infer the film composition and thickness. The RBS spectra were analyzed by the Rutherford backscattering manipulation program (RUMP) [43].

Results and discussion

In order to test the influence of the deposition parameters on the physical properties of each film, microstructural investigations are of paramount importance, also to obtain a deeper understanding of the film macroscopic properties. Electrical and optical analyses can give information about the film crystalline properties through the steepness of the transmittance spectrum near the fundamental absorption edge, transparency, reflectance, and tailing behavior of the absorption coefficient as well as changes in carrier concentration and mobility [44]. However, the investigation of the crystallographic features, such as texture, crystallite size and shape, lattice parameter, strain effects is the decisive test to correctly interpret important physical properties such as resistivity and optical data. A direct control of the film morphological and structural features is also a basic requirement in order to fully understand the magnetic properties since they depend on dopant uniformity or clustering in the resulting coating as well as the occurrence of localized secondary magnetic phases and dopant segregation at interfaces or GBs. In this respect, high resolution transmission electron microscopy (HRTEM) is a very powerful analysis tool, due to its high sensitivity to detect secondary phase agglomerates, even including few atomic units, at subnanometric resolution.

The RBS spectrum of the LD sample deposited on (100) Si substrate is shown in figure 2. From the RBS analysis it came out that i) the Cr content was sufficient to induce a detectable Cr signal, corresponding to a dopant concentration of 3% and 10%, for the LD and HD, respectively; ii) the thickness of the deposited film was 20 nm within 6%, and iii) the Cr signal indicated an almost uniform depth distribution of the dopant inside the film, for both the doping levels.

The crystalline features and the microstructural details of the deposited samples can be observed in figure 3. Figures 3(a) and 3(b) show the bright field (BF) images of the LD and HD samples, respectively, and figure 3(c) shows the corresponding SAED patterns. From the analyses of the BF images of both samples (figures 3(a) and 3(b)) the following remarks can be inferred: i) the films are formed by large and contiguous crystallites with different crystalline orientation, forming GBs at their intersection; ii) the crystallites have irregular shape and average size of few hundreds of nm; iii) each crystallite exhibits a typical bending-contour contrast, consisting in dark lines, sometimes intersecting and forming a star-like contrast, as shown in the high magnification images reported as inset of figures 3(a) and 3(b); here the details of high symmetry bending contour figures and of the grain boundaries are evidenced; iv) the contrast of these images demonstrates the absence in the films of secondary phases, such as inclusions of metallic chromium or chromium oxides. Concerning the bending-contour contrast, this kind of contrast is generated by a local bending of atomic planes with respect to the direction of the incident electron beam. Due to the crystal bending, the excitation error, i.e. the deviation from the Bragg condition of a given diffracted beam, changes across the crystallite, causing the contrast visible in the BF images. The local bending of the crystal lattice is related to enhanced internal strain and thus to a modification of the elasticity. Comparison between the BF images of the LD and HD samples (figures 3(a) and 3(b)) indicates a preferential alignment and torsion of the GBs as well as lengthening of the polycrystalline foils when dealing with the higher Cr content. As far as the diffraction analysis is concerned, the LD and HD samples exhibited the same features, which are represented by the SAED pattern reported in figure 3(c). The pattern shows spotty rings confirming the polycrystalline nature of the films. The interplanar distances obtained from such diffraction pattern, reported in table I, are in agreement with the corresponding values associated to the cubic bixbyite structure of In_2O_3 (lattice constant of 1.0118 nm) and no trace of secondary phases can be

detected. Therefore, both BF images and SAED patterns indicate that, regardless of the doping level, Cr atoms don't aggregate in the film to form secondary phases, but are included into the ITO matrix, possibly as substitutional atoms. Thus, the internal strain, resulting in the observed bending of the host crystal lattice, is most likely the result of the incorporation of the Cr atoms within the ITO lattice. In fact, i) the low growth temperature as well as the absence of post-deposition thermal annealing rule out strain effects due to film-substrate thermal expansion mismatch and ii) the amorphous substrate avoids the strain components usually induced by film-substrate structural difference and lattice constant mismatch. Since neither thermal strain nor substrate-induced strain component can explain the observed lattice bending, the dopant-induced growth stress is the only remaining strain component.

A careful analysis was devoted to the data derived from both the high resolution images and diffraction patterns in order to point out any possible change of the lattice parameter, since the substitution of the In^{3+} (0.94 Å) cations by the smaller Cr^{3+} ions (0.76 Å) [45] in the lattice sites is expected to decrease the final distances between Cr and their oxygen neighbors after relaxation. In this respect, it must be noticed that lattice contraction would result from relaxing of the dopant-induced strain and strain relaxing is a thickness-dependent effect. Namely, whenever strain effects are induced, a film becomes less and less stable during its growth evolution and the stored elastic density energy is fully released beyond a critical thickness. Since the deposited films are very thin (20 nm), no critical strain gradients and/or partial strain relaxation should occur. Therefore, no significant change of the ITO lattice constant should take place by Cr doping at the present growth stage. Indeed, reduction of the lattice constant could not be evidenced by the high resolution image and diffraction pattern analyses, within the resolution limit of the technique. Further investigations are in progress to ascertain strain-relaxation induced change of the lattice constant for thicker films, while preserving the considered doping levels.

Figures 4(a) and 4(b) report of the high resolution (HRTEM) images obtained from a GB region for the LD and HD samples, respectively. They show completely misoriented grains, as confirmed by the zone axis attributed to each grain, compatible with high angle GBs. Moreover, regardless of the doping level, the grains are in close contact with each other and a certain amount of overlap between contiguous grains can be observed (figure 4(b)). No secondary or amorphous phase is observed at the

GB as well as in the crystallites forming the boundaries, within the detectability limits of the technique. It is worth noting that in the case of the HD sample a single GB between two slightly overlapping grains is visible confirming the preferential alignment and torsion of the GBs at high doping level.

As a further investigation, the high resolution image in figure 5(a) was obtained from the centre of a high symmetry bending-contour figure (see the detail evidenced by an arrow in figure 3(b) of the HD sample). It can be seen that 211 and 002 lattice fringes dominate the contrast of the image. Fast Fourier transform (FFT) was calculated on two different regions of the image (marked with dashed rectangles 1 and 2) obtaining the patterns reported as inset in figures 5(b) (region 1) and 5(c) (region 2). The spots correspond to the main periodicities present in the phase contrast image, and to their vectorial composition; the zone axis is the [120]. By comparing these patterns, it can be noted that the intensities of the spots change, the -211 and 2-1-1 being the most intense of pattern b, and the 004 and 00-4 prevailing in patterns c and d. In the case of the experimental image of figure 5(a), the only parameter which can affect the intensity of the spots is the orientation of the lattice planes with respect to the zone axis direction [120]. Therefore, the intensity change confirms the elastic deformation of the sample which produces a bending of the lattice planes, locally varying the diffraction conditions. The filtered inverse FFTs, reported in figures 5(b) and 5(c), enhance the different phase contrast generated by the crystal bending in the two different areas of the image.

At last, chemical analyses were carried out by EDS technique. In this respect, the electron beam was focused on a suitably selected point of the sample and the X-ray signal was detected, collected and processed. The X-ray photon energy of the peaks detected in the spectra was correlated with the atomic species within the films. Figure 6 reports the EDS spectra obtained from the LD and HD samples; both spectra cover the energy range of interest, namely where the chromium related peaks are expected. It is worth noting that the Cr-K α peak, at 5.41 keV, is scarcely visible in the spectrum of LD sample whereas the same peak results well evident in the spectrum of the HD sample. Its average intensity, obtained from a series of spectra recorded from different points of the sample, is $(7.8 \pm 1.3)\%$ the intensity of the main In-L α peak, at 3.28 keV. Further EDS investigations were performed in order

to show eventual chromium segregation at the GBs, but, in agreement with the BF and HRTEM analyses, no concentration change was detected, within the EDS detection capability.

From the obtained experimental results the following remarks can be inferred: i) taking into account both low-growth temperature and film thickness (only 20 nm), the degree of crystallinity and the complete substrate coverage observed in the films would not be expected. Basically, the transformation from amorphous state to crystalline phase requires the nucleation of critical-size clusters and their subsequent growth as well as improved lattice order. The PLD deposition peculiarities combined with growth parameters optimized as reported in ref. [25,26,28] were surely decisive in determining the onset of crystallization by ad-atom coalescence and attachment at the amorphous/crystalline interfaces. Therefore, the observed crystallinity can be attributed to the hyper-thermal energy-distribution of the PLD-induced deposition flux and to the pulsed nature of the deposition. While the former feature improves the ad-atom superficial mobility, favoring collision events and the probability for more ad-atoms to aggregate even at low substrate temperatures, the latter effect allows that the deposited species spreading over the growing surface before the arrival of the next depositing pulse. The absence of Cr oxides, dopant clusters and segregation at the GBs can be related to the PLD-induced growth kinetics combined with the discussed advantages of the double-target ablation and choice of a metallic target for the dopant. Indeed, the very different doping levels, used for the LD and HD samples, rule out the possibility that just a too low dopant content could have favored dopant dilution. As a further confirmation, the internal strain, resulting in the bending of the host lattice, was detected even for the LD sample and it was observed to increase significantly turning in the HD sample. In this respect, polycrystallinity, size and shape distribution of the crystalline flakes composing the films and their evolution as a function of the doping level suggest combined effect between PLD-enhanced nucleation density and dopant-induced strain gradients. In fact, since the supersaturation of the PLD deposition flux increases the density of nucleation sites, the growth of small contiguous island and their coalescence is favored with respect to the growth of separated and large islands. Furthermore, the smaller Cr ions compared to the In cations introduce lattice-potential fluctuations capable of capturing ad-atoms. That is the increase of the doping level enhances dopant localization effects and dopant effectiveness as nucleation centers. On the other hand, the stored strain

density energy drives the superficial diffusion of the ad-atoms depending on the distribution of the directions and regions of low/high strain. Therefore, the observed preferential alignment and torsion of the GBs as well as the lengthening of the polycrystalline flakes with the increase of the doping level, suggest that the growth is influenced by the Cr-induced strain gradients, namely the growth strain component introduced by defect/dopant. Indeed, both low growth temperature and very thin thickness of our films don't let the material to respond to the stored stress via reduction of the stored strain energy density.

Finally, as a further check of the Cr-induced modification of the host ITO matrix, the sample morphology was investigated by atomic force microscopy (AFM) in contact mode. The average roughness was found to increase from nearly 0.1nm to nearly 0.4-0.5nm.

Summary

In the present paper the structure and compositional features of Cr-doped ITO films grown at room temperature on amorphous silica substrates have been reported and discussed in relation to doping level, film thickness, substrate choice and features of the deposition method. The films crystallize as thin polycrystalline flakes, hundreds of nm wide, forming large angle GBs and exhibit local bending of the crystal lattice caused by Cr-induced internal strain. The lattice structure of the films coincides with the cubic bixbyite structure of ITO, no dopant segregation phenomena and no evidence of secondary phase related to metallic Cr or Cr oxides are found, suggesting the successful incorporation of Cr atoms in the host ITO lattice. The degree of crystallinity observed in the films, despite of the low growth temperature (RT) and their very low thickness (20 nm), is explained by the peculiar growth kinetics allowed and involved by the PLD technique combined with the used efficient doping method, namely the double-target ablation using a metallic pellet as dopant source.

Acknowledgements

The authors acknowledge the useful assistance and support of Dr. E. Piscopiello and Mr. M. Palmisano during the TEM analyses at the Tecnai G2 laboratory at the ENEA UTS Center in Brindisi.

References

- [1] Ohno H, 1998 Science 281, 951
- [2] Dietl T, Ohno H, Matsukura F, Cibert J and Ferrand D 2000 Science 287, 1019
- [3] Awschalom D D, Loss D, Samarth N (Eds.) 2002 *Semiconductor Spintronics and Quantum Computation* (Springer, Berlin)
- [4] Dietl T 2006 Materials Today 9, 18
- [5] Awschalom D D and Flatté M E 2007 Nature Physics 3, 153
- [6] Ohno Y, Young D K, Beschoten B, Matsukura F, Ohno H and Awschalom D D 1999 Nature 402, 790
- [7] Dery H, Dalal P, Cywiński Ł and Sham L J 2007 Nature 447, 573
- [8] Davis A H and Bussmann K 2003 J. Appl. Phys. 93, 7358
- [9] Bergenti I, Dediu V, Arisi E, Mertelj T, Murgia M, Riminucci A, Ruani G, Solzi M and Taliani C 2004 Org. Electron. 5, 309
- [10] Shikoh E, Fujiwara A, Ando Y and Miyazaki T 2006 Jpn. J. Appl. Phys. 45, 6897
- [11] Hamberg I and Granqvist C G 1986 J. Appl. Phys. 60, R123
- [12] Philip J, Punnoose A, Kim B I, Reddy K M, Layne S, Holmes J O, Satpati B, Leclair P R, Santos T S and Moodera J S 2006 Nat. Mater. 5, 298
- [13] Dietl T 2003 Nature 2, 646
- [14] Singh R K and Narayan J 1990 Phys. Rev. B 41, 8843
- [15] Wilmot P R and Huber J R 2000 Rev. Mod. Phys. 72, 315
- [16] Eason R 2007 *Pulsed Laser Deposition of Thin Films* (Wiley-Interscience Robert Eason ed.)
- [17] Zheng J P and Kwok H S 1993 Thin Solid Films 232, 99
- [18] Adurodija F O, Izumi H, Ishihara T, Yoshioka H, Matsui H and Motoyama M 1999 Jpn. J. Appl. Phys. 38, 2710
- [19] Aziz M J 2008 Appl. Phys. A 93, 579

- [20] Kim H and Gilmore M 1999 J. Appl. Phys. 86, 6451
- [21] Kim H, Horwitz J S, Kushto G, Pique A, Kafafi Z H, Gilmore C M and Chrisey D B
2000 J. Appl. Phys. 88, 6021
- [22] Qiao Z, Latz R and Mergel D 2004 Thin Solid Films 466, 250
- [23] Korotcenkov G, Brinzari V, Cemeavski A, Ivanov M, Golovanov V, Cornet A, Moraine
J, Cabot A and Arbiol J 2004 Thin Solid Films 460, 315
- [24] Jung Y S 2004 Solid State Commun. 129, 491
- [25] Ngaffo F F, Caricato A P, Fazzi A, Fernandez M, Lattante S, Martino M and Romano F
2005 Appl. Surf. Sci. 248, 428
- [26] Lattante S, Romano F, Caricato A P, Martino M and Anni M 2006 Appl. Phys. Lett. 89,
031108
- [27] Adurodija F O, Semple L and Brünig R 2006 J Mater. Sci. 41, 7096
- [28] Ngaffo F F, Caricato A P, Fernandez M, Martino M and Romano F 2007 Appl. Surf. Sci.
253, 6508
- [29] Giusti G, Tian L, Jones I P, Abell J S and Bowen J 2009 Thin Solid Films 518, 1140
- [30] Kumar D, Apte P R and Pinto R 1995 J. Appl. Phys. 77, 5802
- [31] Freibert F, Cao G, McCall S, Shepard M and Crow J E 1996 J. Appl. Phys. 79, 5876
- [32] Li Y P, Liu J R, Cui C T, Qu J Z, Chen Q Y and Chu W K 1997 Appl. Phys. Lett. 70,
3029
- [33] Low B L, Xu S Y, Ong C K, Wang X B and Shen Z X 1997 Supercond. Sci. Technol. 10,
41
- [34] Xu S Y, Ong C K, Zhou Y L, Low B L, Chen L F and Zhang X 1998 Physica C 297, 43
- [35] Ong C K, Xu S Y and Zhou W Z 1998 Rev. Sci. Instrum. 69, 3659
- [36] Li J, Huang Q, Li Z W, You L P, Xu S Y and Ong C K 2001 J. Appl. Phys. 89, 7428
- [37] Liu X H, Chen S J, Li M and Wang X D 2007 Thin Solid Films 515, 6744
- [38] Muto H, Asano T, Wang R P and Kusumori T 2005 Appl. Phys. Lett. 87, 162106

- [39] Arnold C B and Aziz M J 1999 Appl. Phys. A 69, S23
- [40] Kim J H, Lee S and Im H S 1999 Appl. Surf. Sci. 151, 6
- [41] Grigorescu C E A *et al.* 2003 Appl. Surf. Sci. 212, 78
- [42] Williams J E, Camata R P, Fedorov V V and Mirov S B 2008 Appl. Phys. A 91, 333
- [43] Doolittle L R 1985 Nucl. Instrum. Meth. B9, 344
- [44] Caricato A P, Cesaria M, Luches A, Martino M, Maruccio G, Valerini D, Catalano M, Cola A, Manera M G, Lomascolo M, Taurino A and Rella R 2010 Appl Phys A 101, 753
- [45] Shannon R D 1976 Acta Crystallogr. A 32, 751

Table Captions

Table 1: Interplanar distances estimated from the diffraction pattern in figure 3(c) and the corresponding values of the cubic bixbyte structure of In_2O_3 .

Figure Captions

Figure 1: PLD experimental set-up using a double-target carousel

Figure 2: RBS spectrum of the LD sample

Figure 3: BF TEM images of the LD (a) and HD (b) samples and their typical SAED pattern (c). The numbering of the diffraction spots is related to the indexing of the pattern, reported in Table I

Figure 4: High-resolution TEM images of a typical grain boundary region of the LD (a) and HD (b) films

Figure 5: High-resolution TEM image obtained from a high symmetry bending contour figure of the HD sample (a). FFTs (inset) and filtered inverse FFTs (b, c) obtained from the regions in the dashed rectangles 1 and 2, respectively

Figure 6: EDS spectra obtained from LD (a) and HD (b) samples

Table I

Experimental data		Theoretical data	
N	D _{exp} (Å)	D _{theo} (Å)	hkl
		In ₂ O ₃ cubic*	
1	7.17±0.03	7.155	110
2	5.07±0.02	5.059	200
3	4.13±0.01	4.131	211
4	2.90±0.01	2.921	222
5	2.54±0.01	2.530	400
6	2.39±0.01	2.380	411
7	2.16±0.01	2.157	332
8	1.97±0.01	1.984	431
9	1.79±0.01	1.788	440
10	1.62±0.01	1.599	620
11	1.51±0.01	1.491	631

* ICDD PDF card No. 06-0416

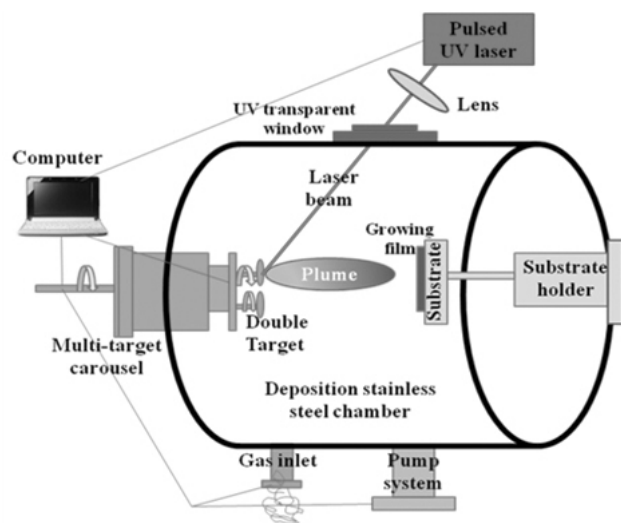


Figure 1: PLD experimental set-up using a double-target carousel

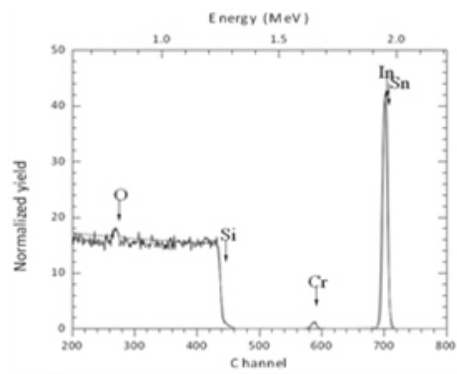


Figure 2. RBS spectrum of the LD sample

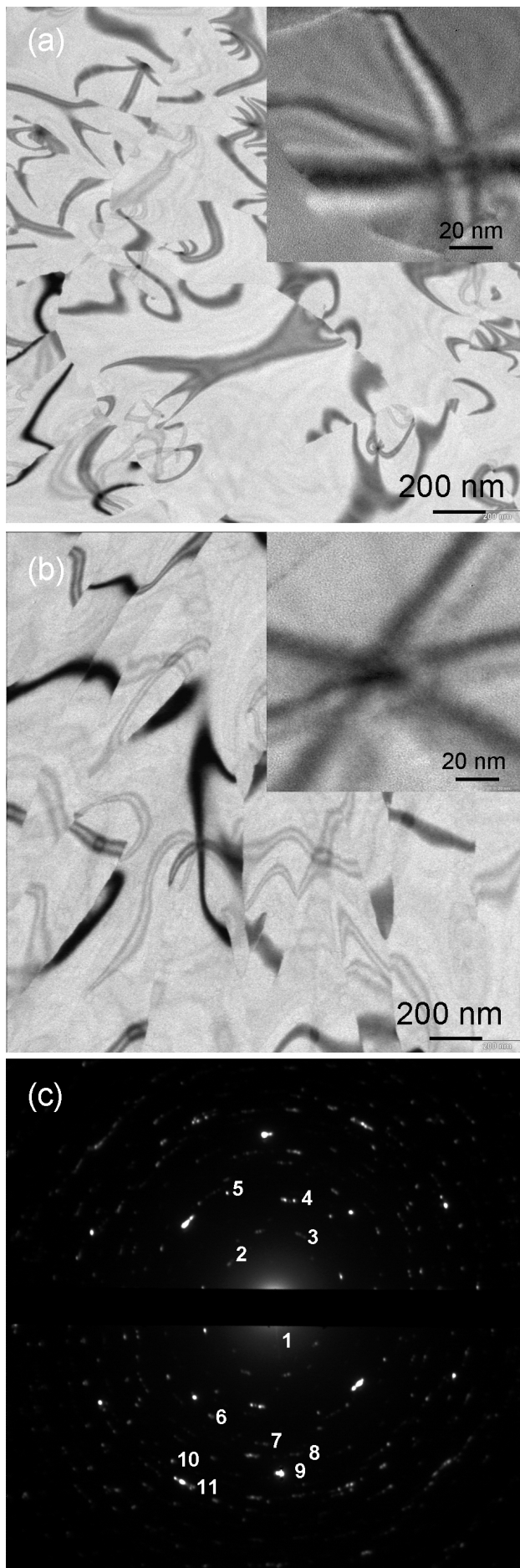


Figure 3: BF TEM images of the LD (a) and HD (b) samples and their typical SAED pattern (c). The numbering of the diffraction spots is related to the indexing of the pattern, reported in Table I

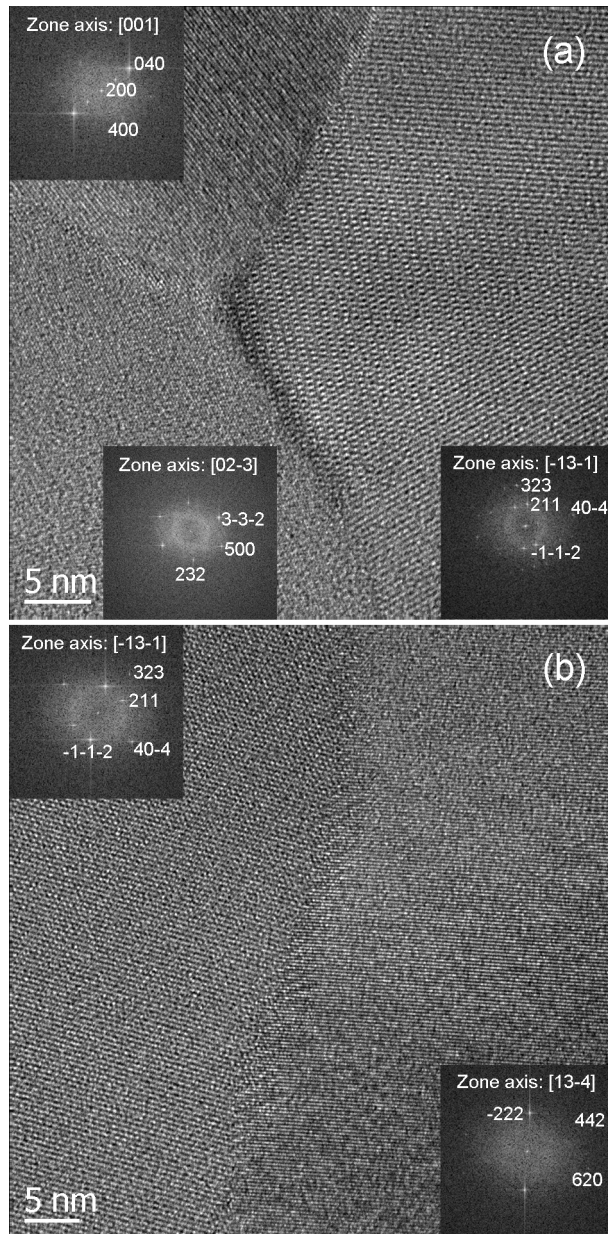


Figure 4: High-resolution TEM images of a typical grain boundary region of the LD (a) and HD (b) films

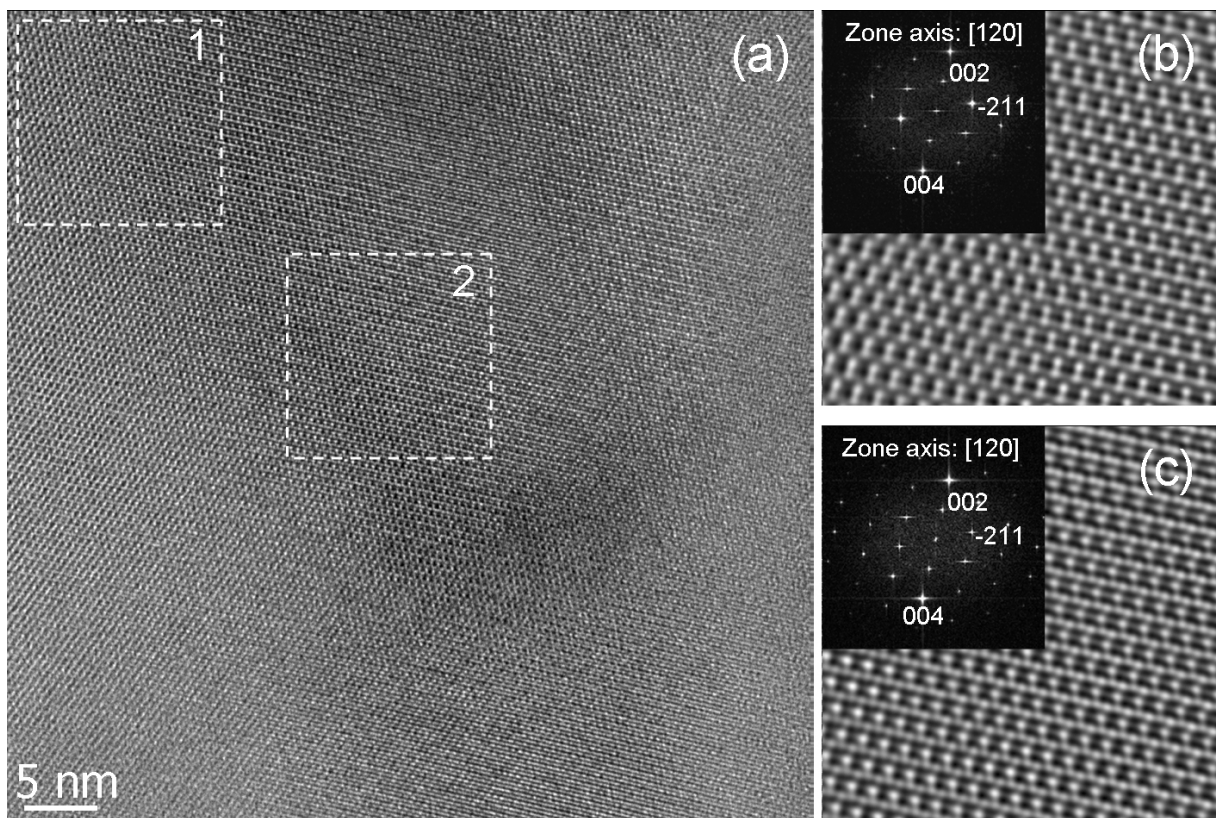


Figure 5: High-resolution TEM image obtained from a high symmetry bending contour figure of the HD sample (a). FFTs (inset) and filtered inverse FFTs (b, c) obtained from the regions in the dashed rectangles 1 and 2, respectively

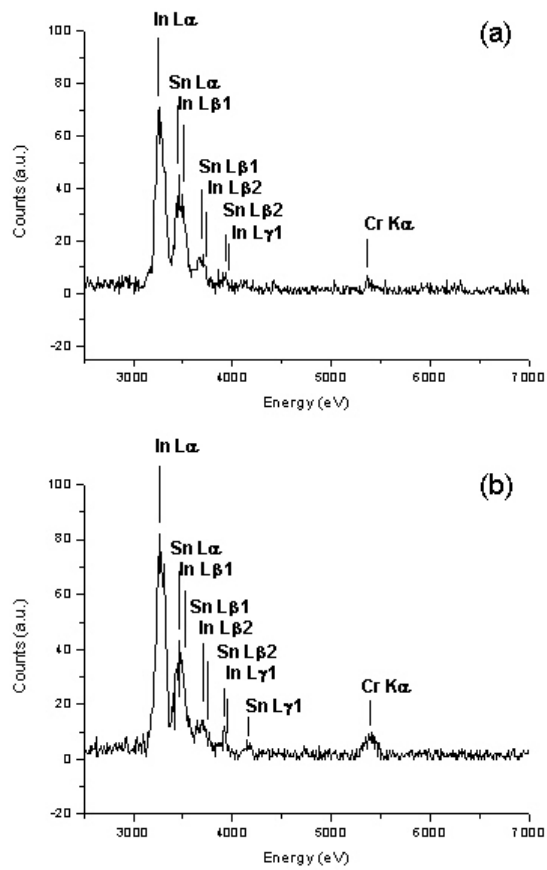


Figure 6: EDS spectra obtained from LD (a) and HD (b) samples